Microstructural Evolution and Magnetic Properties of $NiFe_2O_4$ Nanocrystals Dispersed in Amorphous Silica

Liping Li,[†,§] Guangshe Li,*[,†,‡] R. L. Smith, Jr.,[‡] and H. Inomata[‡]

Physics Department, Jilin University, Changchun 130023, P. R. China, Research Center of Supercritical Fluid Technology, Department of Chemical Engineering, Tohoku University, Sendai 980-8579, Japan, and Department of Materials Science, California Institute of Technology, Pasadena, CA 91125

Received June 13, 2000. Revised Manuscript Received September 5, 2000

$NiFe_2O_4$ nanocrystals were dispersed in silica by a sol−gel route. The dried gel was amorphous, in which isolated Fe^{3+} ions had a weak interaction with silica matrix, as characterized by a weak IR absorption at ca. 580 cm^{-1}. Heat treatment at 400 °C resulted in nickel ferrite clusters being partially formed, and these clusters were observed to interact with the matrix through Si−O−Fe bonds. This interaction reached its maximum with the complete formation of $NiFe_2O_4$ clusters as the temperature was raised to 600 °C. Above this temperature, $NiFe_2O_4$ clusters grew larger into nanocrystals, while the interaction between the nanocrystals and silica matrix disappeared with breakage of Si−O−Fe bonds. The grain growth for magnetic nanoparticles was accompanied with rearrangement of amorphous silica network. The preference of forming $NiFe_2O_4$ nanocrystals eliminated the possibility of precipitation of crystallite component oxides, e.g., NiO, γ-Fe_2O_3, or Fe_3O_4 in amorphous silica matrix, or crystalline silica, e.g., cristobalite or quartz, even when the treatment temperature was 1100 °C. Fe ions in silica glasses were determined by Mössbauer spectroscopy to be present exclusively as Fe^{3+} ions in a high-spin state at octahedral coordination, and the chemical environment of the Fe^{3+} ions seemed to remain unchanged until the nickel ferrite clusters crystallized. The formation mechanism for $NiFe_2O_4$ nanocrystals can be explained in terms of Ni^{2+} ions shifting from the tetrahedral centers to undistorted octahedral sites in the spinel lattice and the partial transformation of FeO_6 octahedron to FeO_4 tetrahedron. The critical dimension for the $NiFe_2O_4$ nanocrystals in silica was detected as ca. 9 nm. Below the critical size, $NiFe_2O_4$ nanocrystals had a superparamagnetic single-domain structure, while the nanocrystals with particle sizes larger than the critical size exhibited bulklike behavior.

Introduction

Magnetic nanocrystalline solids hold great promise for atomic engineering of the materials with functional magnetic properties.[1] Many magnetic clusters or nanocrystals show superparamagnetism[2] due to the thermal fluctuation of the directions of the magnetic moments in single-domain particles below a certain critical size. Magnetic nanocrystals have been extensively applied in magnetic recording medium, information storage, bioprocessing, and magnetooptical devices.[3] Many synthetic routes have been employed to prepare magnetic nanocrystals including sol−gel, coprecipitation, emulsion liquid membrane, and so on.[4] However, nanocrystalline powders prepared by these routes usually have a strong tendency to aggregate, which makes it very difficult to preserve their unique properties.

Nanocomposites could provide an effective solution to this problem, since they can retain the nature of the nanocrystals through dispersion of the nanocrystals in inorganic or organic matrixes. Thus dispersed nanocrystals often possess limited particle agglomeration and narrow grain size distribution under the space confinement effects. The amorphous matrixes have been shown to play an important role in retarding the motion of the particles as well as the grain growth during the formation of nanocrystals. In addition, the morphologies,

* To whom correspondence should be addressed at Tohoku University. E-mail: guangshe@scf.che.tohoku.ac.jp.
† Jilin University.
‡ Tohoku University.
§ Present address: Caltech.

(1) Hirai, T.; Kobayashi, J.; Komasawa, I. *Langmuir* **1999**, *15*, 6291. (b) Kodama, R. H. *J. Magn. Magn. Mater.* **1999**, *200*, 359. (c) Shafi, K. V. P. M.; Koltypin, Y.; Gedanken, A.; Prozorov, R.; Balogh, J.; Lendvai, J.; Felner, I. *J. Phys. Chem.* **1997**, *101B*, 6409.
(2) Eibschutz, M.; Shtrikman, S. *J. Appl. Phys.* **1968**, *39*, 997.
(3) Anton, I.; Dabata, I. D.; Vekas, L. *J. Magn. Magn. Mater.* **1990**, *85*, 219. (b) Gunther, L. *Phys. World* **1990**, *3*, 28. (c) McMickael, R. D.; Shull, R. D.; Swartzendruber, L. J.; Bennett, L. H.; Watson, R. E. *J. Magn. Magn. Mater.* **1992**, *111*, 29.
(4) Courty, P.; Ajot, H.; Macilly, C.; Delmon, B. *Powder Technol.* **1973**, *7*, 21. (b) Niznansky, D.; Viart, N.; Renspinger, J. L. *IEEE Trans. Magn.* **1994**, *30*, 821. (c) Shi, Y.; Ding, J.; Liu, X.; Wang, J. *J. Magn. Magn. Mater.* **1999**, *205*, 249. (d) Yang, J. M.; Tsuo, W. J.; Yen, F. S. *J. Solid State Chem.* **1999**, *145*, 50. (e) Music, S.; Popovic, S.; Dalipi, S. *J. Mater. Sci.* **1993**, *28*, 1793. (f) Walker, E. H.; Breen, M. L, Jr.; Apblett, A. W. *Chem. Mater.* **1998**, *10*, 1265. (g) Elmasry, M. A. A.; Gaber, A.; Khater, E. M. H. *Powder Technol.* **1997**, *90*, 165. (h) Gadalla, A. M.; Yu, H. F. *J. Mater. Res.* **1990**, *5*, 2923. (i) Randhawa, B. S.; Singh, R. *J. Phys. IV* **1997**, *7*, 89. (j) Tu, M.; Shen, J. Y.; Chen, Y. *Thermochim. Acta* **1997**, *302*, 117. (k) Pannaparayil, T.; Marande, R.; Komarneni, S.; Sanker, S. G. *J. Appl. Phys.* **1988**, *64*, 5641. (l) Komarneni, S.; D'Arrigo, M. C.; Leonelli, G.; Pellacani, G. C.; Katsuki, H. *J. Am. Ceram. Soc.* **1998**, *81*, 3041.

10.1021/cm000481l CCC: $19.00
Published on Web 11/22/2000

particle size distribution, and crystal structures for the nanocrystals can be controlled by changing the compositions of the matrixes, concentration, and treatment conditions.[5] It is also shown that nanocrystals dispersed in the matrix provide added advantages to those undispersed nanocrystals.[6]

Many researchers are aware that nanocomposites can be used to stabilize the properties of nanocrystals and are now making great efforts to develop synthetic routes for formation of novel magnetic nanocomposites. Soft chemistry methods are frequently adopted, and rich structural and physical properties have been revealed using matrixes with different compositions. An outstanding feature of nanocomposites is that metastable structures and unusual polymorphs can be achieved by incorporating nanocrystals into the polymers, B_2O_3, P_2O_5, or SiO_2 matrixes. Ziolo et al.[7] prepared isolated metastable γ-Fe_2O_3 in polymer by an ion-exchange resin. Similarly, Ennas et al.[8] stabilized γ-Fe_2O_3 nanocrystals in silica matrix by gelling of tetraethoxysilane and iron(III) nitrate mixture solutions. However, when the nanocomposite was heated to temperatures above 900 °C, γ-Fe_2O_3 particles dispersed in silica glasses were destabilized and transformed into the stable α-Fe_2O_3 phase.[9] It is surprising that, upon heating γ-Fe_2O_3 nanocrystals in a silica aerogel at 1400 °C, a new metastable phase ϵ-Fe_2O_3 can be obtained.[10] Alternatively, Shull and Chatterjee et al.[11] prepared iron metal nanocrystals in silica by reduction of iron containing silica gel in hydrogen and ammonia atmospheres. Therefore, it is expected that the microstructure of magnetic particles can be effectively adjusted in a silica matrix and furthermore that the corresponding physical properties can be controlled. However, there are few systematic studies on structural evolution and its correlated physical properties of the superparamagnetic single-domain particles dispersed in silica matrix, especially when the magnetic nanocrystals have multicomponents. This is probably due to the difficulty in controlling the formation reactions and therefore the composition of the nanocrystals.

For example, magnetic nanocrystals can be prepared by a molten route. However extremely high melting temperatures required for the crystallization of nanocrystals lead to reduction processes involving Fe^{3+} to Fe^{2+}. The superparamagnetic spinel clusters with a formula of $Fe^{3+}(Fe^{3+}_{1.30}Fe^{2+}_{0.55}V_{0.15})O_4$ have been dispersed in silica at a melting temperature of 1450 °C.[12] Komatsu et al.[13] prepared $NiFe_2O_4$ nanocrystals from the molten silicate glasses $50SiO_2 \cdot 30Na_2O \cdot 10NiO \cdot 10Fe_2O_3$ at a slightly lower melting temperature of 1200−1400 °C, but these glasses still contained some percentages of Fe^{2+} ions. In the view of the lower temperature methods that offer many potentially attractive features for materials used in practical applications,[14] we report in this paper on the preparation of $NiFe_2O_4$ nanocrystals from silica matrix by the sol−gel route. It will be shown that stoichiometric $NiFe_2O_4$ nanocrystals can be obtained in silica without reduction processes occurring during the formation reactions.

Nickel ferrite ($NiFe_2O_4$) is a typical soft ferromagnetic material, which crystallizes in a completely inverse spinel structure. When the particle size of this material approaches 10 nm, many microstructural and physical properties have been found such as surface spin disorder,[15] external field enhanced effective anisotropy constant, and anomalous cation ratio at A and B sites in small particles.[16] Therefore, it is very important to study the structural, valence, and coordination variations of ferrite nanocrystals during the dispersion in silica matrixes, which may provide insight on the chemistry of the structural evolution of superparamagnetic single-domain particles and, furthermore, on directing the synthesis of novel magnetic nanocomposites. In this work, we follow the structural evolution of superparamagnetic single-domain $NiFe_2O_4$ nanocrystals that have been dispersed into a silica matrix and correlate this evolution with hyperfine interactions and magnetic properties as they progress through successive heat treatment.

Experimental Section

The $NiFe_2O_4$ nanocrystals were prepared in silica by a sol−gel method as described as follows. To avoid high crystallization temperatures and reduction processes, the selection of the starting chemicals is very important. Here, tetraethyl orthosilicate, $Si(OC_2H_5)_4$ (TEOS, 98% purity), was used as the precursor for silica gel because TEOS is easily hydrolyzed and condensed in the presence of dilute HCl catalyst, giving rise to homogeneous gels that are monolithic and transparent. $Fe(NO_3)_3 \cdot 9H_2O$ (A.R.) and $Ni(NO_3)_2 \cdot 6H_2O$ (A.R.) were employed as the starting iron and nickel species because the decomposition temperature for the nitrate ions is relatively low, i.e., 300 °C. The initial ratios were fixed as $Ni:Fe:SiO_2 = 1:2:9$. First, 2.9 g of $Ni(NO_3)_2 \cdot 6H_2O$ and 8.1 g of $Fe(NO_3)_3 \cdot 9H_2O$ were dissolved in 40 mL of ethyl alcohol and stirred thoroughly in a magnetic stirrer, respectively. Both solutions were added to a given amount of solution containing $Si(OC_2H_5)_4$ and H_2O with a molar ratio of 2:1. The entire mixture was thoroughly stirred for 2 h. A small amount of dilute HCl was added to the solution to act as catalyst and to reduce pH. The wet sol was allowed to gel at room temperature for several days. The gel pieces of the $10(NiO-Fe_2O_3)-90SiO_2$ glasses were then heated at different temperatures for 2 h in air. The transparency of the gel with the composition of $10(NiO-Fe_2O_3)-90SiO_2$ was strongly affected by thermal treatment, i.e., the dried gels grew darker brown in color with increasing temperature. Samples were labeled as S200, S400, S600, ... to indicate heat treatment temperature as 200, 400, 600 °C, ..., respectively.

(5) Pascal, C.; Pascal, J. L.; Favier, F.; Moubtassim, M. L. E.; Payen, C. *Chem. Mater.* **1999**, *11*, 141.
(6) Feltin, N.; Pileni, M. P. *Langmuir* **1997**, *13*, 3927.
(7) Ziolo, R. F.; Giannelis, E. P.; Weinstein, B. A.; Horo, M. P. O.; Ganguly, B. N.; Mehrotra, V.; Russell, M. W.; Huffman, D. R. *Science* **1992**, *257*, 219.
(8) Ennas, G.; Musinu, A.; Piccaluga, G.; Zedda, D.; Gatteschi, D.; Sangregorio, C.; Stanger, J. L.; Concas, G.; Spano, G. *Chem. Mater.* **1998**, *10*, 495.
(9) Viart, N.; Niznansky, D.; Rehspringer, J. L. *J. Phys. IV Colloq.* **1997**, *7* (c1), 555.
(10) Tronc, E.; Chaneac, C.; Jolivet, J. P. *J. Solid State Chem.* **1998**, *139*, 93.
(11) Shull, R. D.; Ritter, J. J.; Swartzendruber, L. J. *J. Appl. Phys.* **1991**, *69*, 5144. (b) Chatterjee, A.; Chakravorty, D. D. D.; Choudhury, K. *Appl. Phys. Lett.* **1990**, *57*, 1360.
(12) Hayashi, M.; Susa, M.; Maruyama, T.; Nagata, K. *J. Electron. Mater.* **1995**, *24*, 983.
(13) Komatsu, T.; Soga, N. *J. Appl. Phys.* **1980**, *51*, 601. (b) Komatsu, T.; Soga, N. *J. Appl. Phys.* **1979**, *50*, 6469. (c) Krystyna, E.; Lipinska, K.; Edward, G. *J. Non-Cryst. Solids* **1988**, *107*, 73. (d) Brooks, J. S.; Williams, G. L.; Alten, D. W. *Phys. Chem. Glasses* **1992**, *33*, 167.
(14) Li, G.; Mao, Y.; Li, L.; Feng, S.; Wang, M.; Yao, X. *Chem. Mater.* **1999**, *11*, 1259. (b) Reddy, C. V. G.; Manorama, S. V.; Rao, V. J. *Sens. Actuators* **1999**, *55B*, 90.
(15) Kodama, R. H.; Berkowitz, A. E.; McNiff, E. J.; Foner, S. *Phys. Rev. Lett.* **1996**, *77*, 394.
(16) Haneda, K.; Kojima, H.; Morrish, A. H. *J. Magn. Magn. Mater.* **1983**, *31−34*, 951.

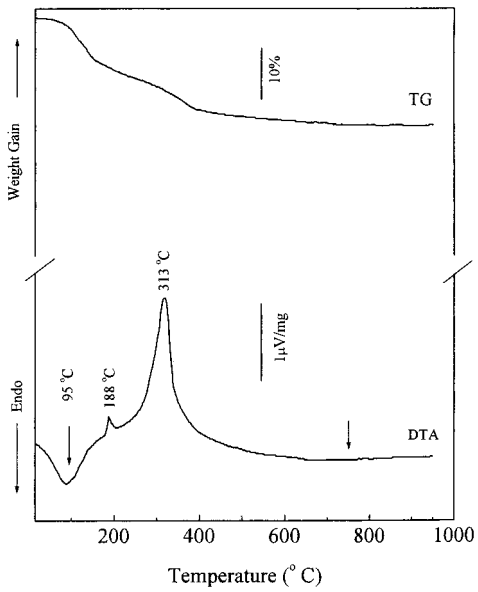

Figure 1. TG-DTA curves for the dried-gel 10($NiO-Fe_2O_3$)−90SiO_2 (S200) measured in air at a heating rate of 20 °C/min.

Simultaneous differential thermal analysis and thermogravimetric (TG-DTA) curves for the samples were recorded on a PE-DTA 1700-TGA7 PC thermoanalyzer in air at a heating rate of 10 °C/min.

The structures for the $10NiFe_2O_4$–$90SiO_2$ composites were identified by means of powder X-ray diffraction (XRD) on a Rigaku, D/max-γA, 12 kW XRD diffractometer with a rotating Cu target at room temperature. The scan rate was 0.3° 2θ/min. Silicon powder (99.99% purity) was used as the standard for peak position determination. The lattice parameters for the samples were refined by least-squares methods. The average grain sizes (D) were measured from the XRD peaks using the Scherrer formula.

The infrared (IR) spectra were recorded on a Nicolet 5DX IR spectrometer on samples pelletized with KBr powder. The magnetization curves for the samples were measured at room temperature by a LD5-9500 vibrating-sample magnetometer.

^{57}Fe Mössbauer spectra were measured at room temperature by means of an Oxford MS-500 constant-acceleration spectrometer. The velocity was calibrated with an α-Fe foil. The radiation sources were ^{57}Co/Rh. The thicknesses of the samples used in the measurements were 3−5 mg of Fe/cm^2.

The electron paramagnetic resonance (EPR) measurements were performed on a Bruker ER200D spectrometer. A frequency of ca. 9.77 GHz was used for a dual-purpose cavity operation. The magnetic field of 0.32 mT was modulated at 100 kHz. A microwave power of ca. 6.5 mV was employed. Reference signals of Mn^{2+} ions in MgO crystals were used as the standard for the precise effective g-factor value. All measurements were carried out at room temperature.

Results

1. Thermal Behavior of the Dried Gel 10($NiO-Fe_2O_3$)−90SiO_2. Figure 1 illustrates the TG-DTA curves measured in air for the dried gel 10($NiO-Fe_2O_3$)−90SiO_2 (S200). In Figure 1, we observed one endothermic peak at 95 °C with a weight loss of ca. 10% and two exothermic peaks at 188 and 313 °C with weight losses of ca. 3% and 8%, respectively. The first peak centered at 95 °C was ascribed to the elimination of the water absorbed in the gel. The two subsequent exothermic peaks at 188 and 313 °C were ascribed to the combustion of the unreacted alkoxide organic ligand[17] and complete decomposition of NO_3^- ions[18] introduced by starting materials. An extremely weak and broad endothermic peak that was observed over the range of 450−850 °C was probably due to the dehydroxylation. It is worth noting that an exothermic peak corresponding to the crystallization of nickel ferrite nanocrystals was not observed. A possible explanation is that the combustion process of the NO_3^- ions overlapped the nucleation process for $NiFe_2O_4$ clusters, and the thermal energy released during the former process further promoted the latter process. This result is different from the undispersed cases, where a strong exothermic peak associated with the transformation from the amorphous to the crystalline nickel ferrite is observed at ca. 400 °C by coprecipitation[19] or at ca. 510 °C by sintering a precursor of Fe_2O_3 coated with $Ni(MEEA)_2 \cdot 0.5H_2O$.[4f]

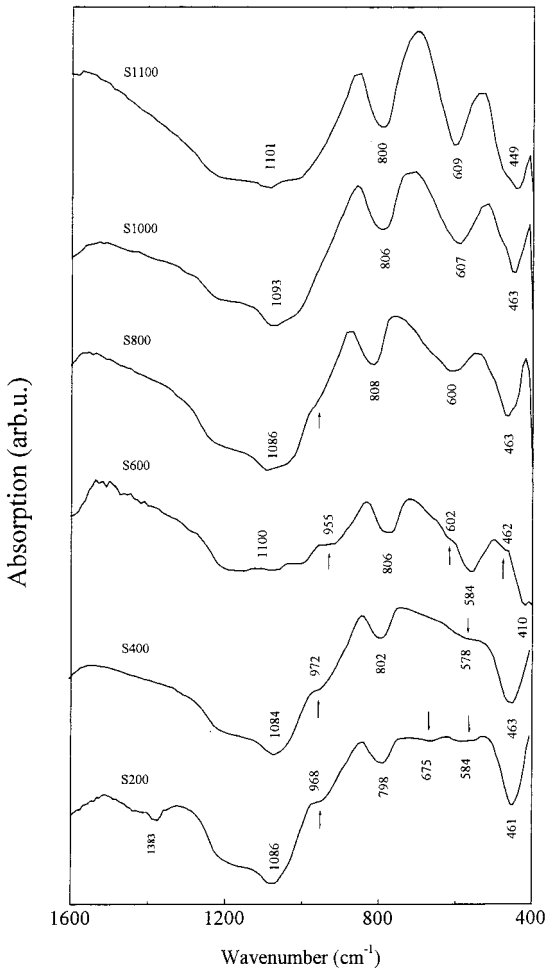

Figure 2. IR spectra for the $NiFe_2O_4$ nanocrystals in SiO_2 obtained by heat treatment of the dried gel at different temperatures.

2. Structural Evolution of $NiFe_2O_4$ Nanocrystals Dispersed in Silica Characterized by IR. Figure 2 shows IR spectra of the $NiFe_2O_4$ nanocrystals that were obtained by heating the dried gel at successively high temperatures. For S200, the broad bands centered at 3420 and 1630 cm^{-1} (not shown) were assigned to the stretching modes and H−O−H bending vibration of the free or absorbed water, while the band at 1383 cm^{-1}

(17) Asomoza, M.; Dominguez, M. P.; Solis, S.; Lara, V. H.; Bosch, P.; Lopez, T. *Mater. Lett.* **1998**, *36*, 249.
(18) Ennas, G.; Mei, A.; Musinu, A.; Piccaluga, G.; Pinna, G.; Solinas, S. *J. Non-Cryst. Solids* **1998**, *232−234*, 587.
(19) Rao, V. S.; Rajendran, S.; Maiti, H. S. *J. Mater. Sci.* **1984**, *19*, 3593.

was assigned to the antisymmetric NO_3^- stretching vibration that is directly related to the residual nitrate groups in the dried gel S200. The characteristic absorptions for the silica network located at 1086, 798, and 461 cm^{-1} were assigned separately as follows: the broad high-intensity band at 1080 cm^{-1} along with the accompanied shoulder at ca. 1200 cm^{-1} was due to the asymmetric LO and TO stretching bonds ≡Si−O−Si≡ of the SiO_4 tetrahedron associated with the motion of oxygen in Si−O−Si antisymmetrical stretch;[20,21] the band at 798 cm^{-1} was assigned to the Si−O−Si symmetric stretch, while the sharp band at 461 cm^{-1} corresponded to the Si−O−Si or O−Si−O bending mode[22] overlapped with the Ni−O stretching vibration. The characteristic absorption for Ni−O bond is given as 466 cm^{-1} in the literature.[23] The shoulder at 968 cm^{-1} was probably composed of the contributions from Si−O−H stretching vibrations[20,22,24] and from Si−O−Fe vibrations.[25] The presence of Si−O−Fe vibrations reflected some interaction between the highly isolated Fe^{3+} ions and the nearest silica matrix. The Si−O−Fe bonds were also evident by the presence of another faint band at 584 cm^{-1}, which was associated with the Fe−O stretching in Si−O−Fe bonds.[25b] Another faint absorption band at 675 cm^{-1} corresponded to the tetrahedral mode of Ni−OH.[26] The presence of Fe−O−Si and Ni−OH bonds sufficiently reflected the chemical nature of the transition metals involved in the dried gel S200. That is, these transition metal ions do not participate directly in the sol−gel chemistry even though they were introduced into the starting solutions in the form of soluble inorganic salts.

For S400, the intensities of the broad bands for the free or absorbed water were drastically weakened, and the characteristic absorption at ca. 1380 cm^{-1} associated with the nitrate species disappeared, which corresponded to the complete decomposition of nitrate species as evidenced by TG-DTA in Figure 1. Other absorptions such as those for silica network remained near the same as those of dried gel S200, while the band for Fe−O stretching in Si−O−Fe bonds at 578 cm^{-1} increased in intensity compared with that for the dried gel S200.

For S600, the absorption band at 1100 cm^{-1} for the ≡Si−O−Si≡ of the SiO_4 tetrahedron was further broadened, while that for Si−O−Si or O−Si−O bending mode at 462 cm^{-1} was much weaker, which corresponded to a rearrangement process of silica network. It should be noted that a new shoulder and a new strong absorption appeared at 602 and 410 cm^{-1}, respectively. Correspondingly, the absorption of the Fe−O stretching band in Si−O−Fe bonds increased. These facts reflected the formation of $NiFe_2O_4$ clusters that was accompanied with the rearrangement of silica network and with the enhancement of the Si−O−Fe bonds between the $NiFe_2O_4$ clusters and the surrounding silica network. It is essential here to emphasize that the composition of the spinel clusters was $NiFe_2O_4$, because in NiO−Fe_2O_3 systems there are two other most possible compounds such as γ-Fe_2O_3 and Fe_3O_4 that could crystallize in the spinel structure with a very similar cell size as that of $NiFe_2O_4$. Gillot et al.[27] studied the transformation of γ-Fe_2O_3 to α-Fe_2O_3 by IR spectroscopy. They found that the transformation was characterized by the disappearance of the IR band at 720 cm^{-1}. However, the IR spectra in Figure 2 do not show this absorption band, suggesting that this γ-phase was not formed in our nanocomposite systems. For Fe_3O_4, there are two characteristic bands,[28] one band at 570 cm^{-1} associated with the Fe−O stretching mode, $v_1(T_{1u})$, of the tetrahedral and octahedral sites and the other band at 370 cm^{-1} associated with the Fe−O stretching mode, $v_2(T_{1u})$, of the octahedral sites. However, Nyquist et al.[29] gave a different absorption center (410 cm^{-1}) for the latter vibration, which is somewhat similar to our IR spectra for S600. As shown by later Mössbauer measurements, no traces of Fe^{2+} were detected. Therefore, the possibility that the spinel clusters contain Fe_3O_4 can be ruled out.

For S800, the IR spectrum changed greatly compared with that for S600. The absorption at 1086 cm^{-1} for ≡Si−O−Si≡ of the SiO_4 tetrahedron grew narrower and stronger, while the shoulder at ca. 960 cm^{-1} became very weak, which was probably due to the lack of the contribution of the Si−O−Fe stretching vibration. The absence of the component from Si−O−Fe vibration at this wavelength can be explained by the broken Si−O−Fe bonds at higher temperatures, which coincided with the disappearance of Fe−O stretching band at 584 cm^{-1} for Si−O−Fe bonds. The band intensity of S800 at 808 cm^{-1} for the Si−O−Si symmetric stretch increased, and the stronger absorption band at 463 cm^{-1} for Si−O−Si or O−Si−O bending mode reappeared. It is interesting to note that both absorptions associated with the characteristic Fe−O and Ni−O stretching modes in $NiFe_2O_4$ phase[30] became much stronger at ca. 600 and 400 cm^{-1}. The breakage of the Fe−O−Si bonds in the interface between the clusters and matrix and the formation of $NiFe_2O_4$ clusters were probably a result of the transformation from FeO_6 octahedron to FeO_4 tetrahedron accompanied with an enhanced covalency of Fe−O bonding.[31]

For S1000, no shoulder was apparent at ca. 960 cm^{-1} for Si−O−H bonds, while the absorption bands for silica matrix network at ca. 1080, 800, and 460 cm^{-1} increased in intensity slightly. The Si−O−Si bridge may have been formed through a polycondensation process. Especially, the broad characteristic Fe−O band for $NiFe_2O_4$ phase at ca. 600 cm^{-1} became much stronger, which

(20) Rao, A. V.; Wagh, P. B.; Haranath, D.; Risbud, P. P.; Kumbhare, S. D. *Ceram. Int.* **1999**, *25*, 505.
(21) Galeener, F. L.; Geissberger, A. E. *Phys. Rev.* **1983**, *B27*, 6199. (b) Burneau, A.; Barres, O.; Gallas, J. P.; Lavalley, J. C. *Langmuir* **1990**, *6*, 1364.
(22) Efimov, A. M. *J. Non-Cryst. Solids* **1996**, *203*, 1. (b) Izutsu, H.; Nair, P. K.; Kiyozumi, Y.; Mizwkami, F. *Mater. Res. Bull.* **1997**, *32*, 1303.
(23) Horanyi, T. S. *Thermochim. Acta* **1989**, *142*, 143.
(24) Scherer G. W. *Relaxation in Glasses and Composites*; Wiley: New York, 1986.
(25) Albawabe, A.; Friberg, S. E.; Sjoblom, J.; Farrington, G. *J. Dispersion Sci. Technol.* **1998**, *19*, 613. (b) Bruni, S.; Cariati, F.; Casu, M.; Lai, A.; Musinu, A.; Picccaluga, G.; Solinas, S. *Nanostruct. Mater.* **1999**, *11*, 573 and references therein.
(26) Clause, O.; Kermarec, M.; Bonneviot, L.; Villain, F.; Che, M. *J. Am. Chem. Soc.* **1992**, *114*, 4709.
(27) Gillot, B.; Jemmali, F.; Rousset, A. *J. Solid State Chem.* **1983**, *50*, 138.
(28) Ishii, M.; Nakahira, M.; Yamanaka, T. *Solid State Commun.* **1972**, *11*, 209.
(29) Nyquist, R. A., Kogel, R. O., Eds. *Infrared Spectra of Inorganic Compounds*; Academic Press: New York, London, 1971.
(30) Kamnev, A. A.; Ristic, M. *J. Mol. Struct.* **1997**, *408/409*, 301.
(31) Rao, G. V. S.; Rao, C. N. R.; Ferraro, J. R. *Appl. Spectrosc.* **1970**, *24*, 436.

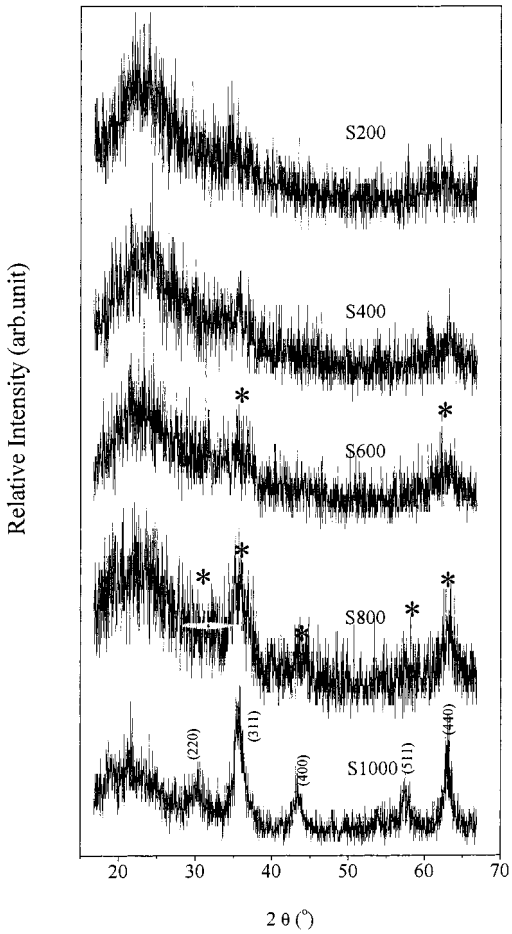

Figure 3. XRD patterns for the $NiFe_2O_4$ nanocrystals in SiO_2 obtained by heat treatment of the dried gel at different temperatures. Asterisks denote the $NiFe_2O_4$ particles.

must correspond to the production of well-crystallized $NiFe_2O_4$ nanocrystals.

For S1100, most of the IR bands remained the same as those of S1000 with the only exception being the band at ca. 600 cm^{-1}, which grew stronger and narrower. This is probably due to a growth process for the large multidomain particles in the $NiFe_2O_4$ phase, which will be discussed in Section 4.

3. Structural Evolution of $NiFe_2O_4$ Nanocrystals Dispersed in Silica Characterized by XRD. Figure 3 illustrates the XRD patterns for the samples after thermal treatment of the dried gel. Both S200 and S400 were characterized by several broad scattering bands similar to those of the amorphous materials, and no obvious Bragg diffraction peaks were observed, indicating that the gels were amorphous below 400 °C. For S600, two new broad peaks appeared at 2θ of ca. 35 and 63°, which correspond to the nucleation of spinel clusters as confirmed by the corresponding IR spectrum, even though the particle size could not be calculated from the XRD peaks due to the very small grain size and low *S*/*N* ratio. However, dispersed peaks of the amorphous silica matrix still existed. For S800, the intensities of both peaks at ca. 35 and 63° further increased, and several new stronger peaks appeared. The positions for these peaks coincided with the characteristic peaks for the standard spinel phase.[32] This confirmed that the cluster size grew into spinel nanocrystals from the silica matrix at 600 °C and the number of the spinel particles increased with increasing temperature. From the broadening effect of the most intense peak (311), the average grain size was determined by Scherrer formula to be ca. 4 nm for the magnetic particles in S800. Similar broadening effect and relatively weak peak intensities have been found in nanocrystalline ferrites.[33]

Further increasing the treatment temperature up to 1000 °C (S1000) resulted in the presence of most of the major peaks matching with standard pattern for bulk $NiFe_2O_4$.[32] The $NiFe_2O_4$ particles precipitated from the silica in S1000 enlarged to ca. 9 nm. For sample S1100, the XRD peaks were slightly stronger than those for S1000 and the particles grew to ca. 13 nm. It should be noted that no traces of quartz, cristobalite, or intermediate products, e.g., Fe_2SiO_4 or Ni_2SiO_4, were formed and only weakening of the peak intensity at ca. 20 ° for the amorphous silica was observed. These results showed that, in these nanocomposite systems, the transition metals did not participate in the direct reaction with the silica matrix and that the crystallization of $NiFe_2O_4$ nanocrystals was accompanied with a rearrangement process of the network for amorphous silica matrix, which was supported by the IR analysis. It is clear that the present results are different from those of the amorphous Fe_2O_3–SiO_2 and NiO−SiO_2 systems.[34] In the latter cases, quartz and cristobalite were formed at temperatures lower than 1100 °C with the diffusion of the Fe^{2+} ions from Fe_2SiO_4 into the unreacted silica network leaving behind SiO_4 groups to form the nuclei of quartz and cristobalite. In some systems, cristobalite can be formed even as low as 950 °C.[35]

4. Structural Evolution of $NiFe_2O_4$ Nanocrystals Dispersed in Silica Characterized by Mössbauer Spectroscopy. The room-temperature Mössbauer spectra for the dried gels after thermal treatment are shown in Figure 4. It is clear that the samples treated at a temperature below 800 °C were in the superparamagnetic states, as characterized by the presence of a single doublet. The hyperfine parameters for the samples are listed in Table 1. From Table 1, it can be seen that the values of isomer shift (IS) for samples S200−S800 were all larger than 0.31 mm/s, indicating that the Fe ions were trivalent in a high-spin state.

It is well-known that, in $NiFe_2O_4$ crystals, Fe ions occupy both octahedral and tetrahedral sites with a similar percentage. Therefore, a transformation process from octahedral to tetrahedral sites can be expected at certain temperatures below the formation temperature of 800 °C for $NiFe_2O_4$ nanocrystals in silica. We propose that, during the coordination change of Fe ions from 6-fold to 4-fold, the FeO_6 octahedron may become seriously distorted, with two of the six Fe−O bonds of the octahedron elongated along an opposite direction while the remaining four Fe−O bonds become shortened. The large distortion of the FeO_6 octahedron is confirmed by the increase of the QS shown in Table 1.

(32) Mclung, W. F., Ed. *Powder Diffraction File: Inorganic Phases;* JCPDS, International Center for Powder Diffraction Data: Swarthmore, PA, 1989; Card No. 10-326.
(33) Ayyub, P.; Multani, M.; Barma, M.; Palkar, V. R.; Vijayaraghavan, R. *J. Phys. C: Solid State Phys.* **1988**, *21*, 2229.
(34) Nanri, H.; Takeuchi, N.; Ishida, S.; Watanabe, K.; Wakamatsu, M. *J. Non-Cryst. Solids* **1996**, *203*, 375. (b) Takeuchi, K.; Isobe, T.; Senna, M. *J. Non-Cryst. Solids* **1996**, *194*, 58.
(35) Wang, L.; Wang, Z.; Yang, H.; Yang, G. *Mater. Chem. Phys.* **1999**, *57*, 260.

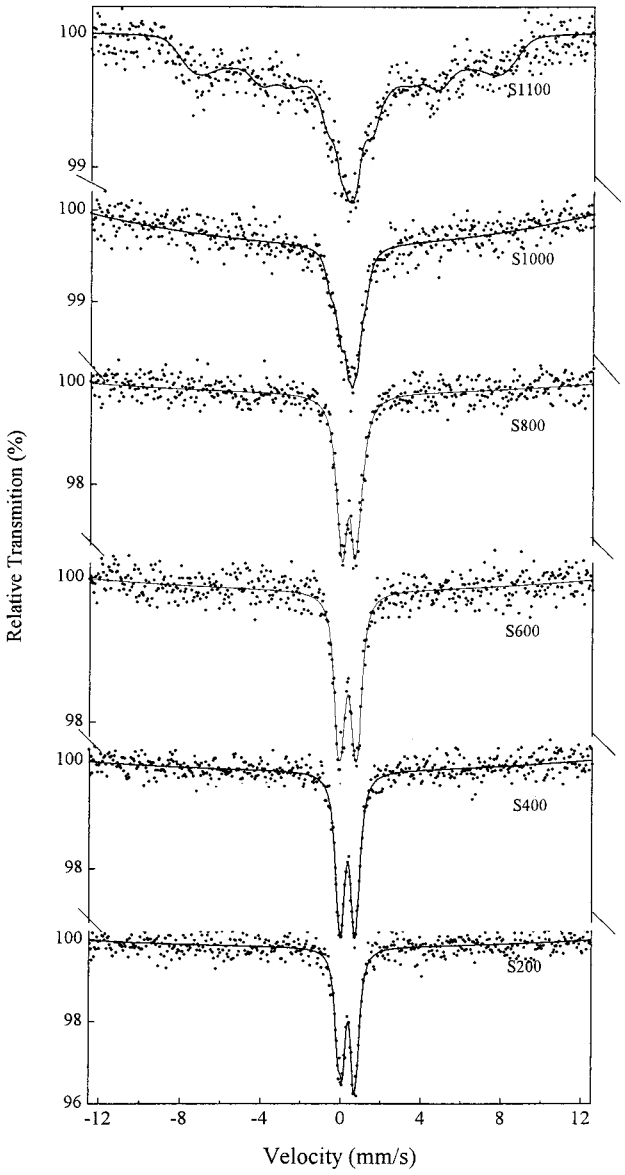

Figure 4. Room-temperature Mössbauer spectra for the $NiFe_2O_4$ nanocrystals in silica obtained by heat treatment of the dried gel at different temperatures.

Subsequently, two elongated Fe−O bonds must have been broken to form the tetrahedron at higher temperatures.

The experimental Mössbauer data for S800 consisted of a single doublet with a broadened width at half-height (Γ). The broadening behavior may hide some complex effects. The structural disorder and paramagnetic relaxation-related phenomena can cause broadening of the absorption width. The IS of ca. 0.33 mm/s for S800 is also larger than that for the tetrahedral Fe ions. The QS reduced ca. 0.13 mm/s compared with that for S600.

For S1000, the Mössbauer spectrum was no longer doublet but an asymmetric broad absorption line. We did not detect any magnetic splitting even though the $NiFe_2O_4$ nanocrystals had precipitated from the silica matrix as observed by XRD. This is evidence that the $NiFe_2O_4$ nanocrystals in S1000 had a critical dimension for superparamagnetism and a very homogeneous particle distribution and that the block temperature for the nanocrystals was below room temperature. At room temperature, the nanocrystals were superparamagnetic. The experimental data for S1000 were fitted by four doublets, giving the smallest χ^2 parameter. The fitting results are shown in Table 1. The components Fe(i) and Fe(ii) with IS > 0.31 mm/s exhibited relative small QS, while the components Fe(ii) and Fe(iv) with IS < 0.26 mm/s possessed relative large QS. We assigned the components Fe(i) and Fe(ii) to the Fe ions in the octahedral and tetrahedral Fe^{3+} on the surface of the nanocrystals $NiFe_2O_4$, while the components Fe(iii) and Fe(iv) to those in the bulk of the nanocrystals. In comparison with the parameters for S200−S800, the octahedral Fe ions in the bulk of $NiFe_2O_4$ nanocrystals of S1000 possessed the smallest QS, whereas those on the surface of the particles exhibited largest QS. The tetrahedral Fe ions in the bulk also gave a QS, 1.05 mm/s. As mentioned above, part of the FeO_6 octahedral appeared to transform into the tetrahedral to yield $NiFe_2O_4$ particles from their respective isolated positions in the amorphous silica matrix. During the transformation process, two Fe−O bonds of the octahedron are probably broken to form the tetrahedron. It is reasonable that the FeO_4 tetrahedron in the bulk had a very large distortion, producing a large QS, 1.05 mm/s. For the tetrahedral Fe ions on the surface of the $NiFe_2O_4$ particles, the large anisotropy effect may have produced a larger distortion of the tetrahedron, accounting for the larger QS, 1.78 mm/s. For the FeO_6 octahedron in the bulk of the particles, the oxygen ions around the Fe ions would probably relax the distortion of the octahedron by high-temperature treatment, leading to the smaller QS of 0.22 mm/s.

In contrast with the variation of QS below 600 °C, the QS of the octahedral Fe ions decreased with increasing treatment temperature above 600 °C. This decrease can be understood in terms of the precipitation and grain growth processes of the $NiFe_2O_4$ nanocrystals. Similar behavior has been found in the $NiFe_2O_4$ particles from molten silica.[13a]

5. Structural Evolution of $NiFe_2O_4$ Nanocrystals Dispersed in Silica Characterized by EPR. EPR is an effective tool for examining the microstructural features of oxide glasses.[36] The X-band EPR spectra in oxide glasses containing Fe ions usually exhibit two well-defined signals of $g_{eff} = 2.0$ and 4.3, which have been considered as a signature for the presence of the Fe^{3+} ions in the glass host. Both signals vary with composition of the glass host, microwave frequency, and temperature. The signal of $g_{eff} = 4.3$ observed in glasses has been ascribed to the isolated Fe^{3+} ions, while the signal of $g_{eff} = 2.0$ has been assigned to the pairs or small clusters of ferric ions. Taking these results into account, two signals of $g = 4.30$ and 2.12 observed in the EPR spectrum for S200 in Figure 5 can be well understood. The signal of $g = 4.30$ reflected the isolated free Fe^{3+} ions, while the large asymmetric signal of $g = 2.12$ was contributed by the Fe^{3+} and Ni^{2+} pairs. These results agreed well with the IR analysis.

At a heat treatment temperature of 400 °C (S400), g_{eff} for isolated Fe^{3+} ions increased slightly to $g = 4.44$ while that as contributed by Fe^{3+} and Ni^{2+} ions decreased to 2.02. Surprisingly, a new signal with $g = 2.26$

(36) Rao, J. L.; Murali, A.; Rao, E. D. *J. Non-Cryst. Solids* **1996**, *202*, 215 and references therein.

Table 1. Hyperfine Parameters for $NiFe_2O_4$ Nanocrystals Dispersed in an Amorphous Silica Matrix

sample	treatment temp. (°C)	isomer shift IS (mm/)	quadrupole splitting QS (mm/s)	half-height width Γ (mm/s)
S200	200	0.357 ± 0.007	0.73 ± 0.01	0.50 ± 0.01
S400	400	0.326 ± 0.006	0.76 ± 0.01	0.52 ± 0.01
S600	600	0.313 ± 0.007	0.85 ± 0.01	0.57 ± 0.01
S800	800	0.328 ± 0.008	0.72 ± 0.01	0.64 ± 0.01
S1000 $Fe(i)_s$	1000	0.31 ± 0.02	0.75 ± 0.04	0.36 ± 0.05
S1000 $Fe(ii)_s$		0.22 ± 0.04	1.78 ± 0.08	0.52 ± 0.05
S1000 $Fe(iii)_b$		0.35 ± 0.01	0.22 ± 0.03	0.38 ± 0.05
S1000 $Fe(iv)_b$		0.26 ± 0.03	1.05 ± 0.06	0.56 ± 0.05

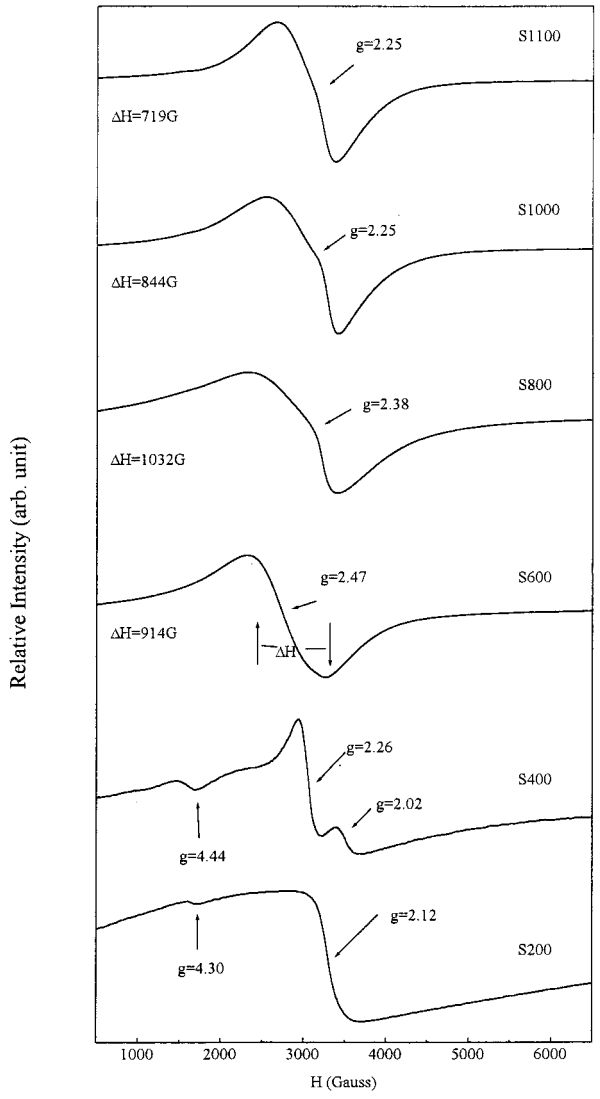

Figure 5. Room-temperature EPR spectra for the $NiFe_2O_4$ nanocrystals in silica obtained by heat treatment of the dried gel at different temperatures. The *g* factors and resonance line widths Δ*H* (left) were obtained by deconvoluting the EPR data.

appeared, which can be ascribed to the formation of $NiFe_2O_4$ clusters.

For S600, the EPR signals associated with the isolated ions disappeared and a new single resonance line was observed. In the spectral analysis, Δ*H* refers to the resonance line width as shown in the figure. This larger *g* factor of 2.47 along with the broad resonance line width Δ*H* of 914 G was an indication of complete formation of $NiFe_2O_4$ clusters and the strong magnetic dipole interactions among these fine clusters. These points will be described in detail in the Discussion (section 3).

For S800, the value of the *g* factor decreased to 2.38, while the line width Δ*H* increased to 1032 G. For S1000 and S1100, the asymmetric EPR signal was constant and had *g* factor of 2.25, while the resonance line width Δ*H* decreased from 844 G for S1000 down to 719 G for S1100. The *g* factor for both samples S1000 and S1100 ($g = 2.25$) was very close to $g_{eff} = 2.21$ for $NiFe_2O_4$ crystals[37] but smaller than $g_{eff} = 2.43$ for polycrystalline $NiFe_2O_4$ powders.[38]

6. Magnetic Properties of the $NiFe_2O_4$ Nanocrystals Dispersed in Silica. Superparamagnetism is often observed for magnetic particles below 10 nm. The occurrence of the superparamagnetism for the present $NiFe_2O_4$ nanocrystals in silica matrix was confirmed by the nearly closed $M-H$ loops as shown in Figure 6 for several samples measured at room temperature. The magnetization did not reach saturation under the present magnetic field. The saturation magnetization was determined by plotting *M* versus *H* and extrapolating to $1/H = 0$. The magnetic parameters for the present samples are plotted in Figure 7. It can be seen that the saturation magnetization increased with the thermal treatment temperature, while the supermagnetism still remained. These results further confirmed the formation of stoichiometric $NiFe_2O_4$ nanocrystals, because, in the Fe_2O_3–SiO_2 nanocomposite system,[8] the transformation of γ-Fe_2O_3 phase to α-Fe_2O_3 at high treatment temperature is accompanied with a decrease in the saturation magnetization and the presence of hysteresis in the magnetization curve.

Discussion

1. Formation Mechanism of $NiFe_2O_4$ Nanocrystals in Amorphous Silica Matrix. $NiFe_2O_4$ nanocrystals were prepared by dispersion in the amorphous silica network. It is interesting to compare results in this study with those obtained from molten synthetic routes[12,13] and in an Fe_2O_3–SiO_2 nanocomposite by a sol–gel method.[25b] For the molten route, the extremely high melting temperatures often introduce reduction processes from Fe^{3+} to Fe^{2+}, which lead to uncontrollable compositions of the nanocrystals. However as mentioned above, for the present work, Mössbauer spectroscopy did not provide any support that such reduction or insertion of Fe^{3+} ions occurred in the silica matrix network. In dried silica gels, a large number of pores exist, and the channels in the silica matrix between adjacent pores are generally very narrow and winding. Bruni et al.[25b] considered that decomposition

(37) Miyamoto, S.; Tanaka, N.; Iida, S. *J. Phys. Soc. Jpn.* **1965**, *20*, 753.
(38) Okamura, T.; Torizuko, Y.; Kozima, Y. *Phys. Rev.* **1952**, *88*, 1425.

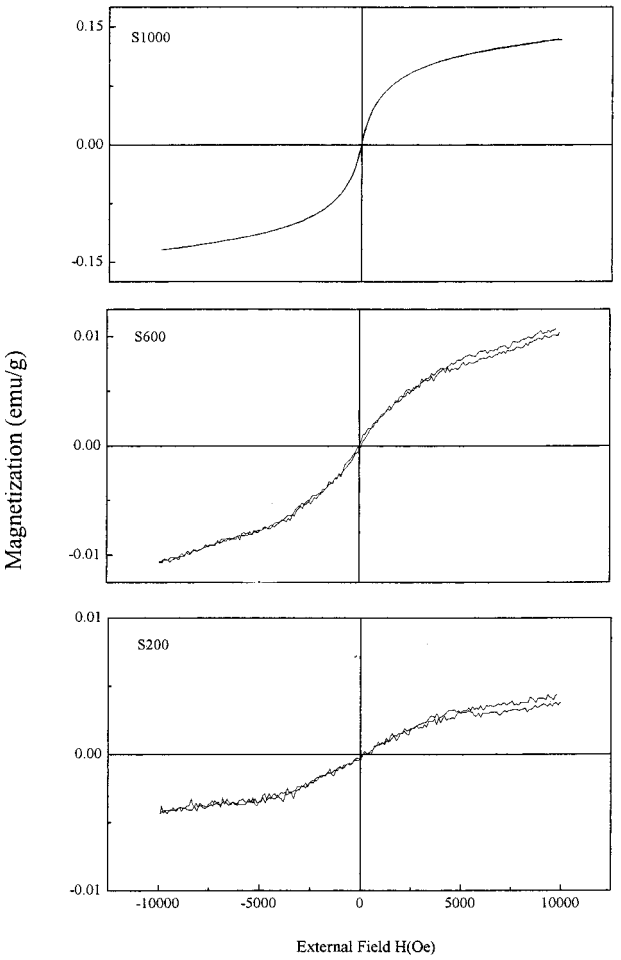

Figure 6. Typical room-temperature magnetization curves for the $NiFe_2O_4$ nanocrystals in silica obtained by heat treatment of the dried gel at different temperatures.

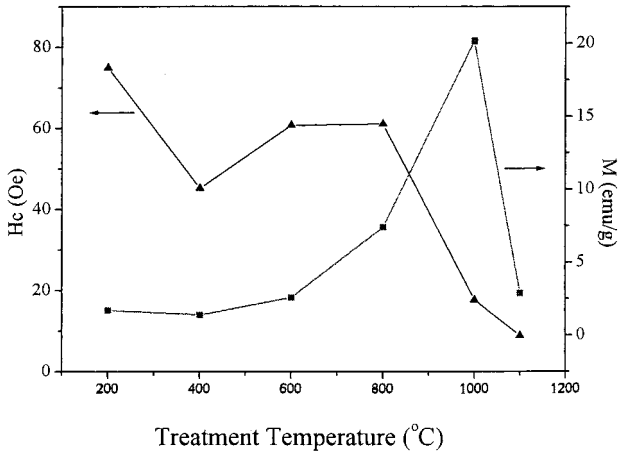

Figure 7. Magnetic properties for the $NiFe_2O_4$ nanocrystals in silica obtained by heat treatment of the dried gel at different temperatures. *M* is saturation magnetization, while Hc is the coercivity.

of the initial iron nitrate in the pores of silica matrix produced Fe_2O_3 nanocrystals in the narrow channels in the silica between adjacent pores. The IR and XRD analyses made in this work did not indicate any traces of Fe_2O_3 or NiO. Therefore, we propose that Fe^{3+} and Ni^{2+} ions do not participate in the direct reaction with the silica matrix but remained in well-isolated pores, where Fe^{3+} ions coordinate with H_2O and NO_3^- or form minor amounts of Fe−O−Si bonds when they become near the silicon atoms at the matrix surface, while Ni^{2+} may coordinate with OH^- and NO_3^- to form a tetrahedron. The Ni^{2+} ions have a large octahedral site preference energy of ca. 21 cal mol^{-1}.[39] Slight changes in the channels in the silica matrix between adjacent pores as promoted by the increased temperature and the combustion of the nitrate groups in the pores probably resulted in partial diffusion of Ni^{2+} and Fe^{3+} in the adjacent pores, allowing them to react with each other and form $NiFe_2O_4$ clusters. However, most Ni^{2+} and Fe^{3+} ions probably remained in their initial isolated pores. Under such low temperatures, the number of $NiFe_2O_4$ clusters formed was very small and therefore undetectable by XRD and IR, but the EPR signal for the clusters was clearly visible. From these results, the EPR signal is more sensitive in detecting the minor chemical reactions that occurred in the silica matrix. The crystallization temperature for $NiFe_2O_4$ powders is ca. 370 °C using liquid metal carboxylates as precursors.[4f] The sluggish reaction for the present $NiFe_2O_4$ particles in silica was most likely correlated with the lower molar ratio of (Ni,Fe) to silica. The pore structure as well as the linked channels should play important roles for formation of single-domain particles. The complete formation reaction for $NiFe_2O_4$ clusters in silica occurred at ca. 600 °C as evident from IR spectra. The clear broadening of the absorption at 1100 cm^{-1} and reappearance of the band at 463 cm^{-1} in the corresponding IR spectra showed a rearrangement process of the silica matrix network. As a result of this rearrangement, the channels linked to the adjacent pores probably became enlarged so as to further promote the complete formation of a large amount of $NiFe_2O_4$ clusters, as characterized by the appearance of only EPR signal of $g = 2.47$ and the absence of the EPR signals for the isolated Fe^{3+} and Ni^{2+}. The extremely small clusters produced very weak XRD peaks in Figure 3. On the other hand, these small clusters had a very large specific surface area, which led to a maximum of interactions with the silica matrix, as characterized by the very strong IR absorption associated with the Si−O−Fe bonds at 584 cm^{-1}. The rearrangement process of the silica matrix from heat treatment apparently promoted the coalescence of $NiFe_2O_4$ clusters into larger nanocrystals. This may be due to the enhanced diffusion of the $NiFe_2O_4$ clusters that is produced by a change in the channels between the adjacent pores.

2. Hyperfine Interactions during Nanocrystal Formation. As shown in Table 1, the IS value decreased while the quadrupole splitting (QS) increased with the increase of treatment temperature from 200 to 600 °C. To understand the variations of these hyperfine interactions, we considered the relationship between both parameters and the electronic density. The IS is proportional to the difference in s-electron charge densities, $e[|\psi_a(0)|^2 - |\psi_e(0)|^2]$, at the nucleus between an absorber and an emitter. The equation for IS can be described as follows:

$$IS = (2/5)\pi Ze^2(R_e^2 - R_g^2)[|\psi_a(0)|^2 - |\psi_e(0)|^2]$$

Here R_e denotes the radii of the excited state and R_g

(39) Komatsu, T.; Soga, N. *J. Mater. Sci.* **1984**, *19*, 2353.

the radii of the ground state. For Fe^{3+} ions, R_e is smaller than R_g. Therefore, the charge density $e|\psi_a(0)|^2$ becomes larger as the value of IS becomes smaller. It should be noted that there are three main factors determining the charge density: (i) valence variation; (ii) $Fe^{3+}-O^{2-}$ distance; (iii) coordination condition. For the nanocomposites produced in this work, the effect from the valence variations is not likely as only Fe^{3+} ions were detected. The electronic density around Fe nucleus in ferric oxides has been calculated theoretically to be a function of the Fe−O distance; that is, charge density $e|\psi_a(0)|^2$ increases with decreasing Fe−O distance.[40] Previous studies[41] also built a relationship between IS and the coordination number of the Fe^{3+} ions. The IS value decreases with the coordination variation of Fe^{3+} ions from octahedral to tetrahedral sites because the 4s electronic density around the Fe nucleus at the tetrahedral site is larger than that at the octahedral site. This results in Fe−O bonding lengths at the tetrahedral site being shorter compared with those at the octahedral site. It is clear that the decrease of IS for these nanocomposite samples at heat treatment below 600 °C corresponds to a formation and growth process of $NiFe_2O_4$ clusters, during which the Fe−O bonding lengths become shortened. Similarly, the average Fe−O distance reduced perceptibly with the grain growth of nanocrystalline Fe_2O_3.[33]

As mentioned above, Mössbauer and magnetic measurements confirmed the superparamagnetic $NiFe_2O_4$ particles dispersed in the silica matrix. It is known that superparamagnetism can induce the collapse of the internal magnetic field. The collapse phenomena for the $NiFe_2O_4$ particles have been studied by Mössbauer technique.[13a,24] Scherer[24] confirmed that 17 nm $NiFe_2O_4$ particles showed ferrimagnetic behavior, whereas 10 nm $NiFe_2O_4$ particles exhibited a superparamagnetic behavior. Komatsu et al.[13a] also found the collapse of the internal magnetic field for 13 nm $NiFe_2O_4$ particles precipitated from a molten silica matrix. For S1000, the internal magnetic field was zero, in accordance with the superparamagnetic $NiFe_2O_4$ particles obtained by others.

3. Magnetic Dipolar Interactions during Nanocrystal Formation. Magnetic dipole interactions among particles and superexchange interactions between the magnetic ions though oxygen ions are two predominant factors that determine the EPR resonance parameters, g factor and resonance line width ΔH. Strong dipole interactions give a large resonance line width and g factor; further, strong superexchange interactions produce a small line width and g factor. Generally, the superexchange interaction should be enhanced when the distance between the magnetic ions and oxygen ions becomes shorter and the corresponding bonding angles are closer to 180°. As mentioned above, after thermal treatment of the gel at 600 °C, large amounts of fine $NiFe_2O_4$ clusters were formed. These clusters had strong magnetic dipole interactions. On the other hand, as shown by the Mössbauer measurements, the FeO_6 octahedron became distorted and some of these transformed into FeO_4 tetrahedra. Therefore, $Fe^{3+}-O-Fe^{3+}$ and $Fe^{3+}-O-Ni^{2+}$ pairs probably have long bond lengths and large deviations of bonding angles from 180°, which will produce weak superexchange interactions among the $Fe^{3+}-O-Fe^{3+}$ and $Fe^{3+}-O-Ni^{2+}$ pairs. The weak superexchange interactions would explain the broadening resonance line width and large g factor observed for S600.

The $NiFe_2O_4$ clusters grew larger into nanocrystals above 800 °C and were accompanied by an increase in crystallinity of the fine particles, as evidenced by XRD in Figure 3. The enhancement of the crystallinity reduced the distortion of the polyhedra in the particles. Correspondingly, the M−O (M = Fe,Ni) bonding length became shorter and the bond angles of these ionic pairs increased toward 180°, causing stronger superexchange interactions among the cations through oxygen ions and a decrease in line width ΔH and g factor. However, as confirmed by our Mössbauer analysis and magnetic measurements, the magnetic particles formed after treatment below 1000 °C were superparamagnetic. The superparamagnetic resonance line width is proportional to the volume of the particles.[42] Therefore, the enlargement of the particle volume with increasing treatment temperature was the primary cause for the broadening of the resonance line width ΔH. As a consequence, ΔH broadened while the g factor decreased for S800 compared with results for S600.

With increasing treatment temperature, the nanocrystals were still in a single-domain structure. The increased particle size should increase the line width, but the distances between the growing particles appeared to weaken interparticle dipole interactions. Particularly, the coordination environments for Fe^{3+} and Ni^{2+} in the well-crystallized nanocrystals tended to be nearly the same as those in the larger crystals, producing very strong superexchange interactions. The network structure for silica matrix should rearrange so as to meet the lowest energy requirement. The final result is the decrease of ΔH and g factor for S1000. We assumed that the $NiFe_2O_4$ particles in S1000 had a critical dimension (ca. 9 nm) for superparamagnetic single-domain structure of $NiFe_2O_4$ particles in amorphous silica matrix. Beyond this dimension, the nanocrystals had enough grain size to show bulk behavior: (i) the value of the g factor remained the same as that ($g = 2.25$) for S1000 but very close to $g_{eff} = 2.21$ for single-crystal $NiFe_2O_4$: (ii) the resonance line width was decreased further to $\Delta H = 719$ G, which is exactly the same as that ca. $\Delta H = 720$ G for nanocrystalline powders $NiFe_2O_4$ (ca. 8.9 nm) by coprecipitation,[43] in which particle agglomeration is readily observed. Therefore, such a powderlike ferrimagnetic resonance in S1100 can be well explained in terms of formation of multidomain structure with partially balanced dipolar fields in the nanocrystals.

4. Correlation of Magnetic Properties with Nanocrystal Formation. The formula for $NiFe_2O_4$ can be well described by $(Fe^{3+})_T[Ni^{2+}Fe^{3+}]_OO_4$, where parentheses and brackets represent the A- and B-site, respectively. In this Neel collinear magnetic structure, the magnetization of the A-sublattice is antiparallel to

(40) Simanek, E.; Stroubek, Z. *Phys. Rev.* **1967**, *163*, 275.
(41) Van Loef, J. J. *Physica* **1966**, *32*, 2102. (b) Stadnik, Z. M.; Zarek, W. *Phys. Rev. B* **1986**, *34*, 1820.
(42) Sharma, U. K.; Waldner, F. *J. Appl. Phys.* **1977**, *48*, 4298.
(43) Sui, Y.; Xu, D. P.; Zheng, F. L.; Su, W. H. *J. Appl. Phys.* **1996**, *80*, 719.

that of the B-sublattice. The net magnetization is therefore dependent primarily upon the nickel magnetic moments while the grain-size dependence of the magnetization reflects the variation of the magnetic interactions during the formation of superparamagnetic single-domain magnetic particles.

The magnetic parameters for the samples are shown in Figure 7. The extremely high Hc for S200 can be explained in terms of the developed anisotropy because the magnetization of smaller magnetic particles is very inhomogeneous.[44] The IR and EPR spectra in Figures 2 and 5 clearly showed the isolated Fe^{3+} and Ni^{2+} ions and the Si−O−Fe bonds. The bonding of these isolated ions to the amorphous silica produced extremely highly local anisotropy fields, which (a) prevent saturation of the magnetization even in very high fields, as found in nanocrystals of $NiFe_2O_4$ coated with organic molecules;[45] and (b) produce very high Hc. The isolated states of Fe^{3+} and Ni^{2+} were broken with increased treatment temperature so as to be distributed in some ordered ways for forming $NiFe_2O_4$ particles. As a consequence, the anisotropy fields were greatly reduced, which accounts for the sudden decrease of Hc for S400. $NiFe_2O_4$ clusters formed completely in S600. The stronger absorption associated with the Si−O−Fe bonds at the clusters−matrix interface at ca. 580 cm^{-1} showed that the interface layer can be taken as a diamagnetic coating on the cluster surface. It is reasonable that the strongly pinned noncollinear structure would develop just as in the case of $NiFe_2O_4$ nanocrystals with organic coatings,[45] which can explain the platform of Hc observed in the temperature interval of 600−800 °C. With further increasing treatment temperatures, these single-domain particles grew to have substantial dimensions which gives bulklike behavior. For this case, the grain size was inversely proportional to Hc.[45] Therefore, Hc decreased in the sequence from S800, to S1000, and to S1100.

The magnetic particles grew with the transformation of the amorphous state to clusters and to single-domain nanocrystals. Correspondingly, the magnetization increased readily (see Figure 7). This trend is in good agreement with theoretical simulations[46] and experimental[44] studies on spherical small magnetic $NiFe_2O_4$ particles. Albuquerque et al.[47] studied the magnetic properties of nanocrystalline NiZn−ferrite−silica systems and found a similar decrease of magnetization for smaller particles, which was closely related to the superparamagnetic relaxation and nonlinearity of the magnetic moment at the surface of the nanocrystals. It is well-know that when the particle size is near to or larger than the critical dimension, the single-domain nanocrystals begin to show bulklike behavior and in these larger particles the superexchange interactions become drastically enhanced, which further reduce the magnetization of the B-site sublattice; therefore, an obvious decrease in the total magnetization can be expected. It is possible to confirm these interactions by introducing lower spin ions into the B-site sublattice to substitute for the higher spin Fe^{3+} ions ($S = 5/2$) because the interactions between the A- and B-site ions can be thus weakened and, as a consequence, the magnetic exchange field at the A-site Fe^{3+} ions is decreased. Indeed, Sankpal et al.[48] observed a decrease in the magnetization of $Ni_{0.7}Zn_{0.3}Fe_{2-x}Cr_xO_4$, where Cr^{3+} ions having a spin of 3/2 were substituted for B-site Fe^{3+} ions. For the present nanocomposite systems, the magnetization referring only to the magnetic nickel ferrite particles after subtracting the weight of the silica matrix is still lower than that (ca. 50 $emu.g^{-1}$) for the corresponding bulk $NiFe_2O_4$. This is closely related to the nonmagnetic amorphous silica layers around the surface of the $NiFe_2O_4$ particles, which leads to the significant decrease of magnetization. Similar phenomena have been found in the smaller $NiFe_2O_4$ coated with organic surfactants.[49]

Conclusions

The microstructural evolution of $NiFe_2O_4$ nanocrystals dispersed in amorphous silica was followed with IR, XRD, Mössbauer, and EPR spectroscopies. Hyperfine interactions and magnetic properties could be correlated with the microstructural evolution brought about by heat treatment of the nanocrystals dispersed in silica matrix at successively higher treatment temperatures. Above 400 °C, $NiFe_2O_4$ clusters and nanocrystals formed in sequence from the silica matrix, accompanied with the rearrangement of silica network. The interaction between the magnetic clusters and silica matrix reached a maximum at a treatment temperature of 600 °C. Above this temperature, the bonding of Fe^{3+} to the silica matrix was broken. All Fe ions exist exclusively as Fe^{3+} ions in a high-spin state either in the silica matrix or $NiFe_2O_4$ nanocrystals. The formation of $NiFe_2O_4$ nanocrystals was probably the result of the shift of Ni^{2+} ions from tetrahedral centers to undistorted octahedral site and the partial transformation of FeO_6 octahedron to FeO_4 tetrahedron. The magnetic nanocrystals below the critical dimension exhibited superparamagnetic behavior at room temperature. The variation of magnetic properties observed is closely related to the magnetic interactions developed with the formation of $NiFe_2O_4$ nanocrystals in silica.

Acknowledgment. This project was financially supported by a fund from NSFC (Grant No.19804005) (L.L.) of P. R. China.

CM000481L

(44) Morrish, A. H.; Haneda, K. *J. Appl. Phys.* **1981**, *52*, 2496.
(45) Berkwitz, A. E.; Lahut, J. A.; Buren, C. E. U. *IEEE Trans. Magn.* **1980**, *Mag-16*, 184.
(46) Wildpaner, V. *Physica* **1975**, *80B*, 346.
(47) Albuquerque, A. S.; Ardisson, J. D.; Macedo, W. A. A. *J. Magn. Magn. Mater.* **1999**, *192*, 277.
(48) Sankpal, A. M.; Surgavanshi, S. S.; Kakatkar, S. V.; Tengshe, G. G.; Patil, R. S.; Chaudhari, N. D.; Sawant, S. R. *J. Magn. Magn. Mater.* **1998**, *186*, 349.
(49) Berkwitz, A. E.; Lahut, J. A.; Buren, C. E. V. *IEEE Trans. Magn.* **1980**, *Mag-16*, 184.